Mechanics Research Communications 52 (2013) 101–107

Contents lists available at ScienceDirect

Mechanics Research Communications

journal homepage: www.elsevier.com/locate/mechrescom

On shear thinning fluid flow induced by continuous mass injection in porous media with variable conductivity

Valentina Ciriello[a,1], Sandro Longo[b,2], Vittorio Di Federico[a,*]

[a] Dipartimento di Ingegneria Civile, Chimica, Ambientale e dei Materiali (DICAM), Università di Bologna, Viale Risorgimento 2, 40136 Bologna, Italy
[b] Dipartimento di Ingegneria Civile, Ambiente Territorio e Architettura (DICATeA), Università di Parma, Parco Area delle Scienze 181/A, 43124 Parma, Italy

ARTICLE INFO

Article history:
Received 12 June 2013
Received in revised form 8 July 2013
Accepted 10 July 2013
Available online xxx

Keywords:
Non-Newtonian
Porous medium
Injection
Similarity solution
Variable permeability

ABSTRACT

A new formulation is proposed to examine the propagation of the pressure disturbance induced by the injection of a time-variable mass of a weakly compressible shear thinning fluid in a porous domain with generalized geometry (plane, radial, or spherical). Medium heterogeneity along the flow direction is conceptualized as a monotonic power-law permeability variation. The resulting nonlinear differential problem admits a similarity solution in dimensionless form which provides the velocity of the pressure front and describes the pressure field within the domain as a function of geometry, fluid flow behavior index, injection rate, and exponent of the permeability variation. The problem has a closed-form solution for an instantaneous injection, generalizing earlier results for constant permeability. A parameter-dependent upper bound to the permeability increase in the flow direction needs to be imposed for the expression of the front velocity to retain its physical meaning. An example application to the radial injection of a remediation agent in a subsurface environment demonstrates the impact of permeability spatial variations and of their interplay with uncertainties in flow behavior index on model predictions.
© 2013 Elsevier Ltd. All rights reserved.

1. Introduction

The mechanics of non-Newtonian fluid flow in porous media has attracted substantial attention in the past and present, as many fluids injected in natural or man-made porous formations exhibit a complex rheological nature (Savins, 1969; Barenblatt et al., 1990; Shenoy, 1995; Chhabra et al., 2001; Sochi, 2010). The range of applications spans extraction of crude oils, underground oil displacement, well drilling, aquifer contamination, soil remediation. The specific nature of the fluid involved governs the choice of a constitutive equation describing the relationship between stress and strain; often the fluid rheological behavior is properly described by a Cross or Carreau–Yasuda model with multiple parameters, but can be approximated in a certain range of shear rates by the simpler two-parameter Ostwald–DeWaele model. At the other end of the spectrum, flow in porous media of viscoelastic liquids or suspensions of long molecular particles entails the adoption of more complex models such as Rivlin–Ericksen second grade (Jordan and Puri, 2003) or dipolar fluids (Puri and Jordan, 2006, and references therein). Adoption of a rheological model at the fluid mechanics scale results in a relationship between pressure gradient and specific flux at the Darcy scale. For power-law fluids, this macroscopic motion equation is particularly simple, and reduces to a nonlinear modification of Darcy's law, often derived using a capillary representation of the porous medium (Cristopher and Middleman, 1965; Teeuw and Hesselink, 1980; Pascal and Pascal, 1985; Pearson and Tardy, 2002). Coupling the motion equation with mass balance yields a transient nonlinear advection–diffusion equation, whose solution gives the pressure in the domain of interest. A particular subclass of analytical solutions to these nonlinear problems is derivable upon adopting a self-similar transformation (Barenblatt, 1996), which yields elegant closed-form results for infinite porous domains subject to different initial and boundary conditions. For free-surface, gravity-driven flow in porous media, examples of this approach are Pascal and Pascal (1993), Bataller (2008), Di Federico et al., 2012a,b. For confined flow, Pascal (1991a,b) studied the pressure perturbations generated in an infinite homogeneous porous domain by an instantaneous mass injection in plane or axisymmetric geometry. Their solution was later extended to spherical geometry by Di Federico and Ciriello (2012), while performing a sensitivity analysis on the results.

The objective of this study is to extend the solution developed by Di Federico and Ciriello (2012) in two respects: (i) allowing for a time variable fluid injection as opposed to an instantaneous one, the former being more suitable in many instances to represent e.g. the continuous release of a displacing fluid, environmental contaminant or remediation agent in the subsurface; (ii) to take into account the combined effect of domain heterogeneity by allowing the porous medium permeability to monotonically vary with the

* Corresponding author. Tel.: +39 051 2093750; fax: +39 051 6448346.
E-mail addresses: valentina.ciriello3@unibo.it (V. Ciriello), sandro.longo@unipr.it (S. Longo), vittorio.difederico@unibo.it (V. Di Federico).
[1] Tel.: +39 051 2093753.
[2] Tel.: +39 0521 905157.

0093-6413/$ – see front matter © 2013 Elsevier Ltd. All rights reserved.
http://dx.doi.org/10.1016/j.mechrescom.2013.07.006

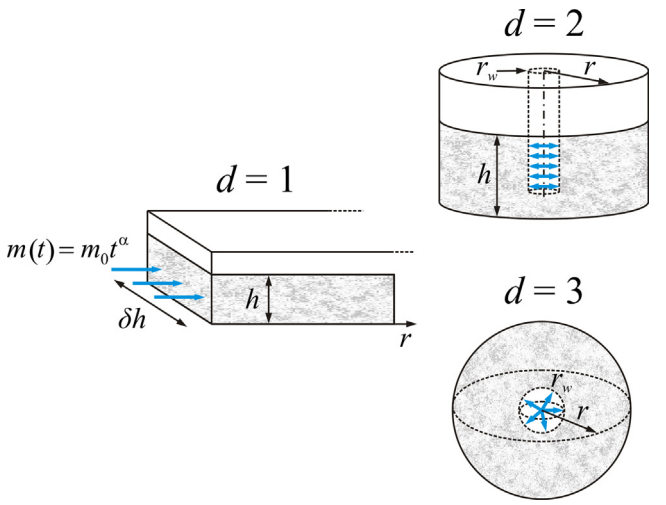

Fig. 1. Domain schematic for plane ($d=1$), cylindrical ($d=2$), and spherical ($d=3$) geometry.

distance from the injection point; such an assumption may represent flow in a domain in which previous injection or pumping has gradually modified the permeability field around the release point in a systematic way. The insight gained may be employed in numerical models of non-Newtonian fluid flow at different scales.

The exposition is organized as follows. The mathematical problem is formulated in Section 2 for a generalized geometry, and solved in Section 3 in self-similar form. Section 4 discusses the limits existing on problem parameters by virtue of formulated assumptions, and their relationship. An application involving the migration of a remediation agent in a subsurface domain is presented in Section 5. Concluding remarks are formulated in Section 6.

2. Problem formulation

A non-Newtonian fluid is injected into an infinite porous domain, initially saturated by another ambient fluid. The propagation of pressure within the domain is taken to be a one-dimensional transient process in plane ($d=1$), cylindrical ($d=2$) and spherical ($d=3$) geometry (Fig. 1). The mass of intruding fluid, injected in the domain origin starting at time $t=0$, increases with time as $m_0 t^\alpha$, with m_0 (dimensions $[MT^{-\alpha}]$) and α being constants; $\alpha=0$ corresponds to the instantaneous release of a given mass, $\alpha=1$ to a constant flux. The domain is described geometrically by its thickness h for $d=1$, 2, and by the surface of the injection zone, equal to δh^2 for $d=1$ (δ being the aspect ratio of the rectangular injection area), $2\pi h r_w$ for $d=2$, and $4\pi r_w^2$ for $d=3$, with r_w being the radius of the injecting well for $d=2$, 3.

The permeability of the porous domain varies in the direction of propagation according to

$$k(x) = k_0 \left(\frac{r}{r^*}\right)^\beta, \tag{1}$$

k_0 being the reference permeability at the length scale r^* and β a real number (Mathunjwa and Hogg, 2007); for $\beta=0$ the porous domain has homogeneous permeability k_0, while for $\beta>0$ and $\beta<0$ the permeability respectively increases or decreases with distance from the injection point. A permeability decreasing with distance from the injection well was considered by Altunkaynak and Sen (2011), while for viscous gravity currents in channels of given shape, the channel width was allowed to vary with distance from the source according to a relation akin to (1), to represent widening or narrowing channels (Takagi and Huppert, 2008). The injected fluid is described by the rheological power-law model, given for simple shear flow by $\tau = \tilde{\mu}\dot{\gamma}\left|\dot{\gamma}\right|^{n-1}$, in which τ is the shear stress, $\dot{\gamma}$ the shear rate, $\tilde{\mu}$ the fluid consistency index and n the flow behavior index (a positive real number); $n<1$ represents shear thinning, $n>1$ shear thickening behavior. The equation of motion for the fluid is a nonlinear modification of Darcy's law, verified experimentally by Cristopher and Middleman (1965) and Yilmaz et al. (2009). Flow and continuity equation read respectively (gravity effects are neglected in spherical geometry):

$$v = \left(-\frac{k(r)}{\mu_{ef}}\frac{\partial p}{\partial r}\right)^{1/n}, \tag{2}$$

$$\frac{1}{r^{d-1}}\frac{\partial}{\partial r}\left(r^{d-1}v\right) = -c_0\phi\frac{\partial p}{\partial t}, \tag{3}$$

where r is the spatial coordinate, t the time, v the Darcy velocity, p the pressure, $c_0 = c_f + c_p$ the total compressibility coefficient, c_f the fluid compressibility coefficient, c_p the porous medium compressibility coefficient, ϕ the porosity, k the permeability coefficient, and μ_{ef} the effective viscosity, given by (Shenoy, 1995)

$$\frac{k}{\mu_{ef}} = \frac{1}{2\tilde{\mu}C_t}\left(\frac{n\phi}{3n+1}\right)^n\left(\frac{50k}{3\phi}\right)^{(n+1)/2}, \tag{4}$$

where $C_t = C_t(n)$ denotes a tortuosity factor for which different expressions are available; in the following, the expression proposed by Pascal and Pascal (1985), i.e. $C_t = \left(25/12\right)^{(n+1)/2}$, will be adopted.

Substituting Eq. (2) in Eq. (3) one obtains:

$$\frac{1}{r^{d-1}}\frac{\partial}{\partial r}\left(r^{d-1}\left(-\frac{\partial p}{\partial r}\right)^{1/n}\right) = -c_0\phi\left(\frac{\mu_{ef}}{k}\right)^{1/n}\frac{\partial p}{\partial t}, \tag{5}$$

with initial condition (p_0 is the ambient pressure)

$$p(r, t=0) = p_0, \tag{6}$$

while conservation of mass $m(t)$ released into the domain requires

$$m(t) = m_0 t^\alpha = \omega h^{3-d}\rho\phi\cdot c_0\int_0^{r_N(t)}(p-p_0)\cdot r^{d-1}\,dr, \tag{7}$$

where ρ is fluid density. In Eq. (7), the factor ω takes the values δ for plane, 2π for radial, and 4π for spherical geometry ($d=1$, 2, 3 respectively) and $r_N(t)$ denotes the advancing compression front. Under the validity of (3), i.e. moderately compressible fluids (for large compressibility coefficients, additional terms arise, see Pascal and Pascal, 1990), it has been demonstrated earlier for a variety of boundary conditions and a homogeneous domain (Pascal and Pascal, 1985; Di Federico and Ciriello, 2012; Ciriello and Di Federico, 2012) that for shear thinning fluids, the front has finite velocity $u(t) = \phi dr_N/dt$, while for Newtonian and shear thickening fluids, no pressure front exists, and $r_N(t)\to\infty$ for any t. Hence for $n<1$ the appropriate boundary conditions are

$$p(r_N(t), t) = p_0, \tag{8}$$

$$\left(\frac{\partial p}{\partial r}\right)(r = r_N(t)) = 0, \tag{9}$$

$$r_N(0) = 0. \tag{10}$$

Dimensionless variables are then defined as follows:

$$(R, H, R_N, T, P, P_0, V, U, M_0) = \left(\frac{r}{r^*}, \frac{h}{r^*}, \frac{r_N}{r^*}, \frac{t}{t^*}, \frac{p}{p^*}, \frac{p_0}{p^*}, \frac{vt^*}{r^*}, \frac{ut^*}{r^*}, \frac{m_0 t^{*\alpha}}{\rho r^{*3}}\right), \tag{11}$$

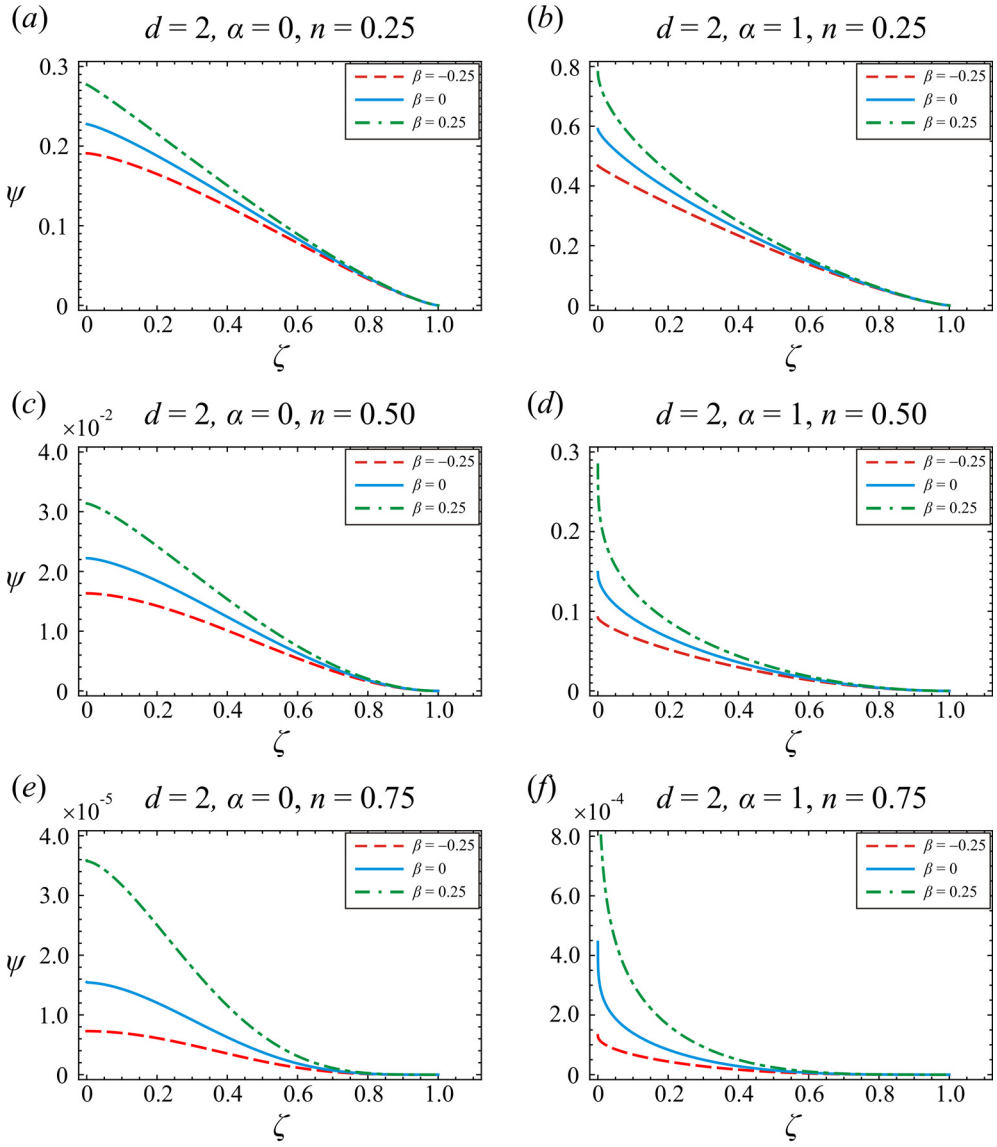

Fig. 2. Shape factor Ψ as a function of dimensionless rescaled similarity variable ζ for cylindrical geometry ($d = 2$); results are shown for $n = 0.25, 0.50, 0.75$ (upper, intermediate, and lower row) and $\alpha = 0$, 1 (left and right column), with $\beta = -0.25$, 0, 0.25.

where r^* is the length scale earlier defined, $p^* = 1/c_0$ the pressure scale, and t^* the timescale; the latter is given by

$$t^* = (\tilde{\mu}^{1/n} r^{*(n+1)/n} / p^{*1/n} k_0^{(n+1)/2n}). \tag{12}$$

With the help of Eq. (4) and the tortuosity expression, this recasts Eqs. (2) with (1) and (5), respectively, in the following dimensionless forms:

$$V = \frac{\phi}{A} R^{\beta(n+1)/2n} \left(-\frac{\partial P}{\partial R} \right)^{1/n}, \tag{13}$$

$$\frac{1}{R^{d-1}} \frac{\partial}{\partial R} \left(R^{F_1} \left(-\frac{\partial P}{\partial R} \right)^{1/n} \right) = -A \frac{\partial P}{\partial T}, \tag{14}$$

where

$$\chi_n = \frac{8^{(1+n)/2}}{2} \left(\frac{n}{3n+1} \right)^n, \quad A = \frac{\phi^{(n+1)/2n}}{\chi_n^{1/n}}, \tag{15a,b}$$

$$F_1 = d - 1 + \beta(n+1)/2n. \tag{16}$$

Eqs (6) and (8)–(10) expressing initial and boundary conditions are formally unchanged, except that dimensionless quantities (in capital letters) replace dimensional ones. The condition given by Eq. (7) becomes instead

$$\Lambda_0 T^\alpha = \int_0^{R_N(T)} (P - P_0) \cdot R^{d-1} dR, \quad \Lambda_0 = \frac{M_0}{\omega H^{3-d} \phi}. \tag{17a,b}$$

3. Solution to the problem

A self-similar transformation is adopted to solve the mathematical problem; first, the scalings $P \approx R^{(\beta-2)(n+1)/[2(n-1)]} / T^{n/(1-n)}$ and $PR^d \approx T^\alpha$ are adopted, as suggested by (14) and (17a) respectively; then eliminating P yields the scale of the pressure front as $R \approx T^{F_2}$, while eliminating R gives $P \approx T^{F_3}$, with

$$F_2 = \frac{2[\alpha(1-n)+n]}{2[1+d+(1-d)n]-(n+1)\beta},$$

$$F_3 = \frac{\alpha(2-\beta)(n+1)-2dn}{2[1+d+(1-d)n]-(n+1)\beta}. \tag{18}$$

The similarity variable is defined as

$$\eta = \frac{A^{F_4} R}{T^{F_2}}, \tag{19}$$

$$F_4 = \frac{2n}{2[1+d+(1-d)n]-(n+1)\beta}, \tag{20}$$

and the similarity solution takes the form

$$R_N(T) = \eta_N A^{-F_4} T^{F_2}, \tag{21}$$

$$P(R,T) = P_0 + A^{dF_4} T^{F_3} f(\eta), \tag{22}$$

where the constant $\eta_N(\alpha, \beta, \Lambda_0)$ denotes the value of η at the pressure front, and the prefactors in (19) and (22) have been inserted to render subsequent equations simpler. Thus (14) and (17a) become respectively

$$\frac{d}{d\eta}\left(\eta^{F_1}\left(-\frac{df}{d\eta}\right)^{1/n}\right) = F_2 \eta^d \frac{df}{d\eta} - F_3 \eta^{d-1} f, \tag{23}$$

$$\Lambda_0 = \int_0^{\eta_N} \eta^{d-1} f \, d\eta, \tag{24}$$

while the conditions at the pressure front (8) and (9) become

$$P(\eta_N) = P_0, \quad \left(\frac{dP}{d\eta}\right)(\eta_N) = 0. \tag{25a,b}$$

Rescaling η as $\zeta = \eta/\eta_N$ and $f(\eta)$ as $f(\eta) = \eta_N^{F_5} \Psi(\zeta)$, where

$$F_5 = \frac{(2-\beta)(n+1)}{2(1-n)}, \tag{26}$$

the final expression for the pressure becomes

$$P(R,T) = P_0 + A^{dF_4} T^{F_3} \eta_N^{F_5} \Psi(\zeta). \tag{27}$$

Substituting these expressions in the governing equations yields the following ordinary nonlinear differential equation in the shape function $\Psi(\zeta)$

$$\frac{d}{d\zeta}\left(\zeta^{F_1}\left(-\frac{d\Psi}{d\zeta}\right)^{1/n}\right) = F_2 \zeta^d \frac{d\Psi}{d\zeta} - F_3 \zeta^{d-1} \Psi, \tag{28}$$

with boundary conditions

$$\Psi(1) = 0, \quad \left(\frac{d\Psi}{d\zeta}\right)(1) = 0, \tag{29a,b}$$

while the position of the moving pressure front is given by

$$\eta_N = \left(\frac{1}{\Lambda_0}\int_0^1 \zeta^{d-1}\Psi(\zeta) d\zeta\right)^{-\frac{2(1-n)}{2[1+d+(1-d)n]-(n+1)\beta}}. \tag{30}$$

For an instantaneous injection ($\alpha = 0$), Eqs. (28)–(30) are amenable to the closed-form solution (note that $F_2(\alpha=0) = F_4$)

$$\Psi(\zeta) = B(1-\zeta^{(2-\beta)(n+1)/2})^{1/(1-n)},$$

$$\eta_N = \left[\frac{\Lambda_0}{BE}\right]^{\frac{2(1-n)}{2[1+d+(1-d)n]-(n+1)\beta}}, \tag{31a,b}$$

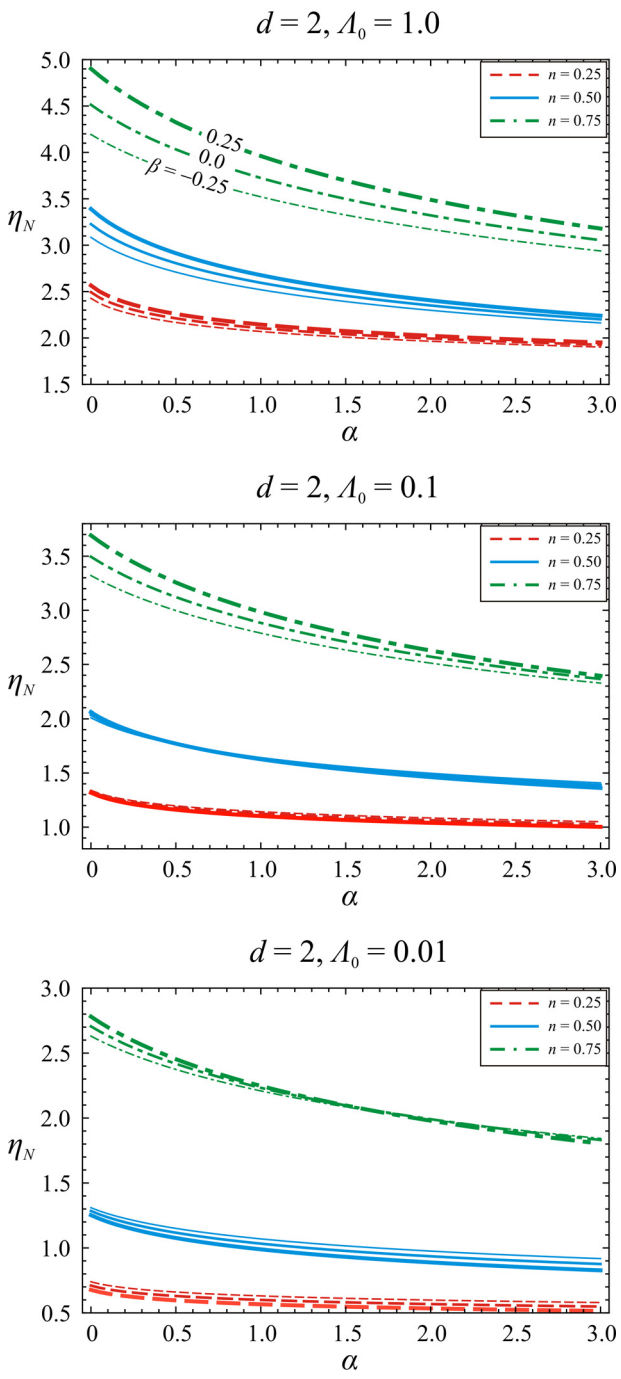

Fig. 3. Prefactor η_N as a function of α for cylindrical geometry ($d = 2$) for $n = 0.25$, 0.50, 0.75, $\Lambda_0 = 1$, 0.1, 0.01 (upper, intermediate, and lower panel), with $\beta = -0.25$, 0, 0.25.

$$B = \left[\frac{2(1-n)F_4^n}{(2-\beta)(n+1)}\right]^{1/(1-n)}, \tag{32}$$

$$E = \frac{2}{2[1+d+(1-d)n]-(n+1)\beta} \times \frac{\Gamma\left(\frac{2d}{(2-\beta)(n+1)}\right)\Gamma\left(\frac{1}{1-n}\right)}{\Gamma\left[\frac{2[1+d+(1-d)n]-(n+1)\beta}{(2-\beta)(n+1)(1-n)}\right]}, \tag{33}$$

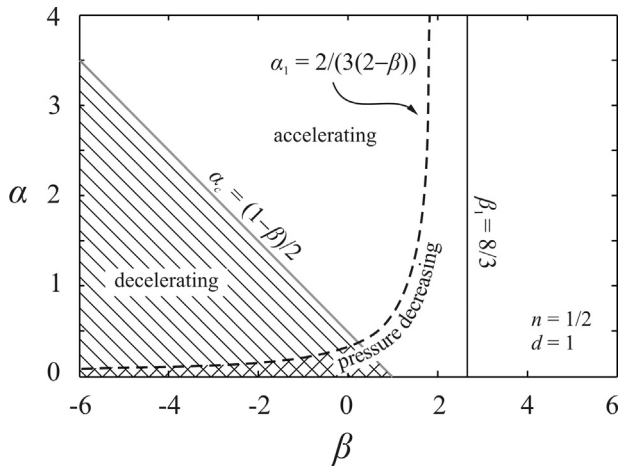

Fig. 4. Constraints placed on problem parameters by model assumptions for $n = 0.50$, $d = 1$.

in which $\Gamma(\cdot)$ is the gamma function. For $\beta = 0$, (31a,b)–(33) reduce to expression reported in Di Federico and Ciriello (2012).

The integration of (28) is performed numerically using Wolfram Mathematica® 7. The resulting shape factors $\Psi(\zeta)$ are depicted in Fig. 2a-f as a function of the dimensionless rescaled similarity variable for cylindrical geometry ($d = 2$); in each figure, results are shown for $\beta = -0.25$, 0, 0.25 over all the possible combinations of $n = 0.25$, 0.50, 0.75 and $\alpha = 0$, 1.

It is interesting to observe that the shape factor decreases significantly for increasing n, while it increases with α for a given fluid as the fluid volume released into the domain increases. In the domain origin, the shape factors show a finite slope for constant volume release ($\alpha = 0$), while for $\alpha \neq 0$ may or may not exhibit a singularity, depending on the interplay amongst parameters d, α, β, and n. Performing the integration also for plane ($d = 1$) and spherical geometry ($d = 3$) (results not shown for the sake of brevity) yields for the constant volume release an inverse proportionality among shape factors and the geometry factor d. For the constant flux release, shape factors are smaller near the origin ($\zeta = 0$) and larger toward the pressure front ($\zeta = 1$) as d increases. The impact of flow behavior index and varying permeability is qualitatively the same for different geometries.

With the same values of rheological index n and permeability variation factor β, and a choice of $\Lambda_0 = 0.01$, 0.1, 1.0, Fig. 3 illustrates the prefactor η_N as a function of α for radial geometry. The behavior of η_N shows throughout lower values for very shear thinning fluids. The dependence of η_N on the value of flow behavior index n is quite significant especially if compared with the modest influence of β in the range examined. Further, as Λ_0 (representing the strength of the injection) increases by an order of magnitude, the prefactor η_N shows a less than proportional increase. Investigation of the behavior of η_N for $d = 1$, 3 (not shown), returns a modest increase with respect to the geometry factor. Numerical results for $\alpha = 0$ perfectly reproduce analytical formulae (31a,b) (comparison not shown).

Once η_N is determined via (30), the pressure field is fully known through (27). The velocity for $\eta < \eta_N$ is then given by

$$V = \phi A^{\frac{(1+d)F_4 - n}{n}} R^{\frac{\beta(n+1)}{2n}} T^{\frac{F_3 - F_2}{n}} \left(-\frac{d\Psi}{d\zeta}\right)^{1/n}. \tag{34}$$

4. Limits of validity

It is noted that for the expression of the distance of propagation of the pressure front $R_N(T)$ to increase with time, it must be

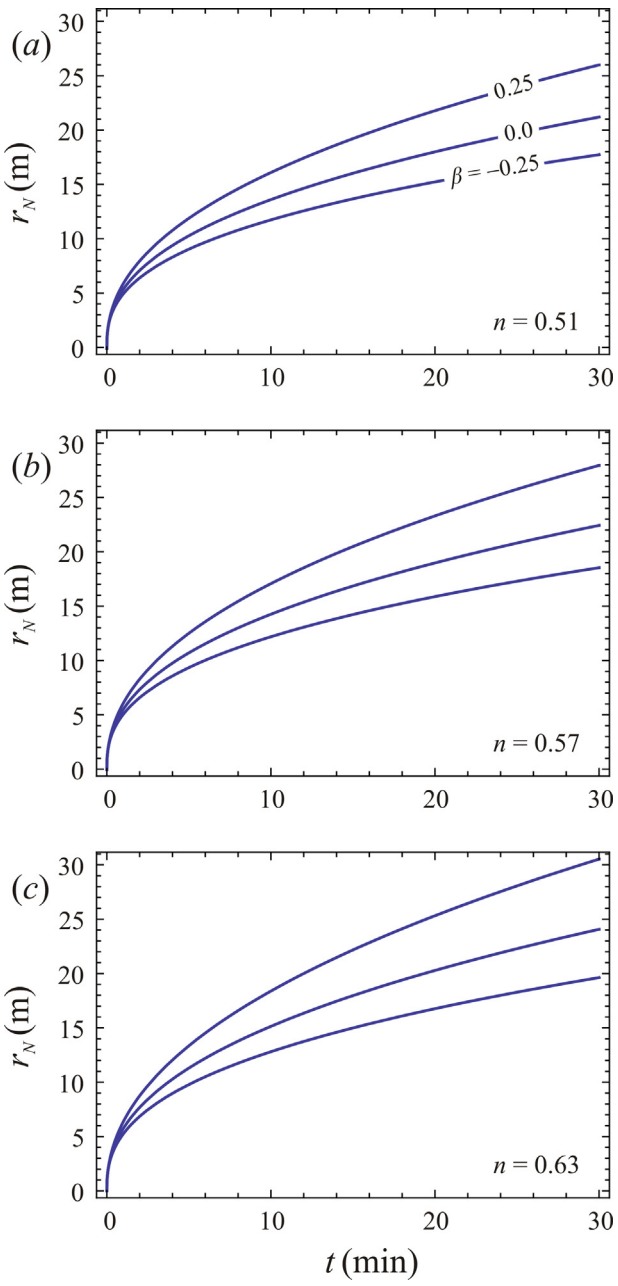

Fig. 5. Position of pressure front r_N versus time t for $d = 2$, $h = 0.33$ m, $\alpha = 1$, $m_0 = 0.5$ kg/s, $\tilde{\mu} = 3.7$ Pa s^n, $\rho = 1000$ kg/m^3, $\phi = 0.49$, $k_0 = 1.1 \times 10^{-9}$ m^2, $c_0 = 2 \times 10^{-8}$ Pa^{-1}, $\beta = -0.25$, 0, 0.25, $r^* = 1$ m, and (a) $n = 0.51$; (b) $n = 0.57$; and (c) $n = 0.63$.

$F_2 > 0$, whence it follows that $\beta < \beta_1 \equiv 2[1 + d + (1 - d)n]/(n + 1) > 2$, which is a positive quantity; this entails an upper limit to the increase of the permeability in the flow direction for the solution to maintain its physical meaning, while no lower limit exists to a permeability decrease. If this condition is respected, it follows that the velocity of the front $U(T) = \phi F_2 A^{-F_4} \eta_N T^{F_2 - 1}$ increases or decreases with time depending whether $0 < \alpha < \alpha_c$ or $\alpha > \alpha_c$, with $\alpha_c = [2(1 + d - nd) - (n + 1)\beta]/[2(n + 1)]$.

Conversely, for given α, the front accelerates or decelerates for $\beta < \beta_c$ or $\beta_c < \beta < \beta_1$, with $\beta_c = [2(1 + d - nd) - (n + 1)\alpha]/(n + 1)$. Upon examining (27), it is seen that at a given point in space the pressure increases, remains constant, or decreases with time depending on whether $F_3 > 0$, $F_3 = 0$, or $F_3 < 0$. Given the previous limit $\beta < \beta_1$, the pressure decreases with time for $0 \leq \alpha < \alpha_1 \equiv 2dn/[(2 - \beta)(n + 1)]$, or, conversely, $\beta_2 = 2 - 2dn/[\alpha(n + 1)] < \beta < \beta_1$. When these inequalities

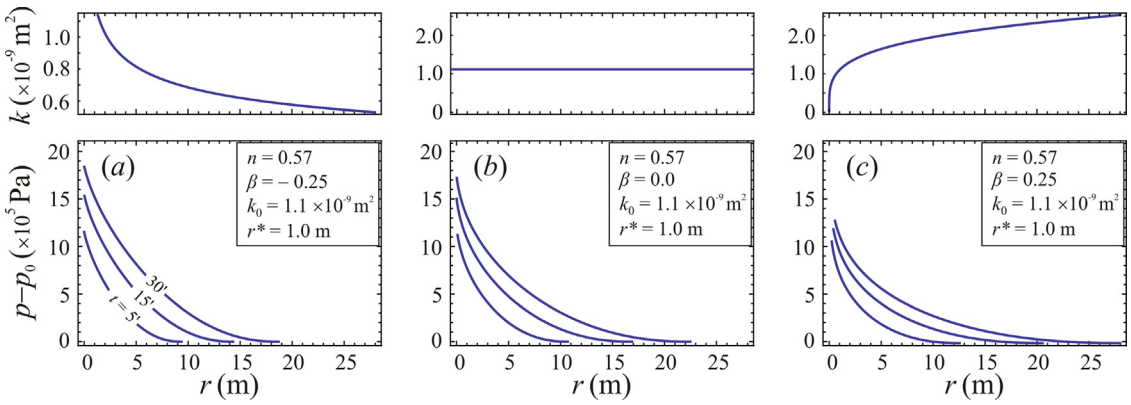

Fig. 6. As Fig. 5 but pressure increment $p - p_0$ versus distance r for $n = 0.57$, $t = 5'$, $15'$, $30'$ and (a) $\beta = -0.25$; (b) $\beta = 0$; and (c) $\beta = 0.25$.

are reversed, the pressure increases with time. Fig. 4 depicts the constraint β_1, the limit for an accelerating front α_c, and the condition for pressure increasing with time α_1, for the selected case $d = 1$, $n = 0.5$. In the hatched domain, the pressure front decelerates, and in the cross-hatched domain also the pressure decreases over time. The picture is qualitatively similar for fluids with different rheological index, with the value of β_1 increasing for decreasing n; the limit values are $\beta_1(n \to 1, d = 1) = 2$ and $\beta_1(n \to 0, d = 1) = 4$. In the latter case $\alpha_1 = 0$ and the domain pressure always increases with time. Analogous results are obtained for different geometries ($d = 2$, 3, not shown).

5. An illustrative example

In this section we illustrate a practical application of our results to injection of a non-Newtonian fluid into a subsurface environment. The geometrical setup and the fluid and domain parameters are derived from Comba et al. (2011), who analyzed the rheological properties of nanoscale iron slurries, which constitute a valuable agent to remediate contaminated aquifers when stabilized through dispersion in xanthan solutions; this produces a fluid with shear thinning characteristics, whose measured apparent viscosity as a function of shear rate and for different values of iron concentration is best described by the four parameter Cross model in the range of shear rates $\dot{\gamma} = 10^{-2}$ to 10^5 s^{-1}.

In the present application, we deduce the two rheological parameters describing a power-law fluid from their measurements for an iron concentration of 30 g/l at intermediate shear rates; the fit is excellent in the range $\dot{\gamma} = 10^{-1}$ to 10^4 s^{-1} and yields $n = 0.57$ and $\tilde{\mu} = 3.7$ Pa s^n. The suspension density is assumed to be $\rho \cong 1000$ kg/m^3. We further consider that a fluid with these characteristics is injected radially ($d = 2$) with a constant ($\alpha = 1$) mass flow rate $m_0 = 0.5$ kg/s (corresponding to the injection flow rate considered in Comba et al. (2011), i.e. 30 l/min) into a domain of height $h = 0.33$ m filled with silica sand, having porosity and reference permeability respectively equal to $\phi = 0.49$, $k_0 = 1.1 \times 10^{-9}$ m^2; the total compressibility is practically coincident with that of the sand and is taken to be $c_0 \cong c_p = 2 \times 10^{-8}$ Pa^{-1}. The problem length scale is fixed to $r^* = 1$ m; the value of r^* is immaterial for a homogeneous medium, but governs the spatial rate of change of the permeability for a heterogeneous one according to (1). Fig. 5b illustrates the position of the pressure front as a function of time for the above parameters and $\beta = -0.25$ (permeability decreasing with distance from injection point), $\beta = 0$ (homogeneous medium), $\beta = 0.25$ (permeability increasing with distance). Fig. 5a and c do the same assuming a 10% error occurred in determining the flow behavior index (i.e. having $n = 0.51$ and $n = 0.63$ respectively), all other parameters remaining equal. It is seen that in a time frame of approximately 30′, the pressure front reaches distances in the range 18–30 m. Cases with $\beta \neq 0$ bring about a variation in the volume of the domain affected by the injection when compared with the constant permeability case; the variation is of order 20%, positive for $\beta > 0$ and negative for $\beta < 0$. An increase in the value of the flow behavior index n implies an increase in the radius of the domain affected; the effects of positive β and larger n are compounded.

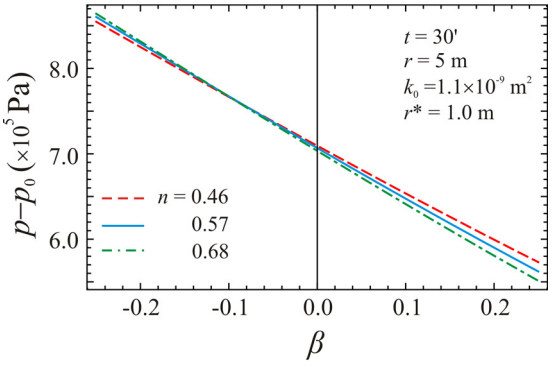

Fig. 7. As Fig. 5 but pressure increment $p - p_0$ versus β for $r = 5$ m, $t = 30'$, $n = 0.57 \pm 0.11$.

Fig. 6a–c shows the pressure behavior versus distance from the injection well for the base value of the flow behavior index $n = 0.57$ and $\beta = -0.25$, 0, 0.25 respectively, at different times $t = 5'$, $15'$, $30'$; the upper panel in each figure depicts the corresponding spatial variation of the permeability. The Figures illustrate the pressure buildup over time with respect to the initial ambient value p_0; this effect is more marked for $\beta < 0$ as the pressure increases more rapidly in the portion of porous domain affected by the injection, given the larger resistance to motion progressively encountered by the fluid; the reverse is true for $\beta > 0$. The behavior of the pressure variation $p - p_0$ over time for values of n smaller or larger than 0.57 demonstrates that a non-monotonic dependence of the pressure from the flow behavior index may exist, but this effect is relatively minor compared to that of the permeability variation. The phenomenon is illustrated in Fig. 7, depicting the pressure variation as a function of β at a radial distance $r = 5$ m and time $t = 30'$ for $n = 0.57 \pm 0.11$; it is seen that a 20% increase in n produces a modest decrease in pressure when β is larger than a threshold value $\beta_t \cong -0.1$; the reverse is true when $\beta < \beta_t$. When different values of r and t are considered, the threshold value changes or does not exist at all.

6. Conclusions

A novel self-similar solution was presented to analyze pressure dynamics induced in an infinite porous medium of generalized

geometry by a continuous mass injection of a power-law shear thinning fluid. The permeability variation along the flow direction was conceptualized as a monotonic power-law variation with distance. Results obtained via a self-similar transformation in dimensionless form generalize earlier findings for an instantaneous injection in a porous medium of uniform permeability, under constraints imposed on model parameters. The existence of a pressure front traveling with a finite velocity is confirmed. The front position and the pressure increment induced in the domain by the injection are functions of geometry, type and intensity of injection, fluid and domain properties. Results may be used as a benchmark for complex numerical models of non-Newtonian fluid flow. An example application to the injection of a remediation agent into the subsurface demonstrates the importance of an accurate determination of the flow behavior index to predict the size of the domain affected by the injection, while the pressure is affected modestly by possible uncertainties in the determination of rheological parameters. Deterministic spatial variations of permeability significantly affect model predictions; their effects interact with variability of the flow behavior index. The high sensitivity of shear thinning fluids to permeability variations was already noted by Sullivan et al. (2006), who conducted pore scale simulations of power-law fluid flow through porous media using lattice Boltzmann techniques. An investigation of the effect of permeability heterogeneity on non-Newtonian flow in a stochastic framework, either with finite (Dagan, 1989) or long-range correlations (Di Federico and Zhang, 1999), constitutes a challenging topic for future research.

References

Altunkaynak, A., Sen, Z., 2011. Steady state flow with hydraulic conductivity change around large diameter wells. Hydrological Processes 25, 1778–1783.

Barenblatt, G.I., 1996. Scaling, Self-Similarity, and Intermediate Asymptotics. Cambridge University Press, Cambridge, UK.

Barenblatt, G.I., Entov, V.M., Rhyzik, V.M., 1990. Theory of Fluid Flows Through Natural Rocks. Kluwer, Dordrecht.

Bataller, R.C., 2008. On unsteady gravity flows of a power-law fluid through a porous medium. Applied Mathematics and Computation 196, 356–362.

Chhabra, R.P., Comiti, J., Machač, I., 2001. Flow of non-Newtonian fluids in fixed and fluidised beds. Chemical Engineering Science 56, 1–27.

Ciriello, V., Di Federico, V., 2012. Similarity solutions for flow of non-Newtonian fluids in porous media revisited under parameter uncertainty. Advances in Water Resources 43, 38–51, http://dx.doi.org/10.1016/j.advwatres.2012.03.028.

Comba, S., Dalmazzo, D., Santagata, E., Sethi, R., 2011. Rheological characterization of xanthan suspensions of nanoscale iron for injection in porous media. Journal of Hazardous Materials 185, 598–605.

Cristopher, R.H., Middleman, S., 1965. Power-law flow through a packed tube. Industrial & Engineering Chemistry Fundamentals 4 (4), 422–426.

Dagan, G., 1989. Flow and Transport in Porous Formations. Springer, New York.

Di Federico, V., Archetti, R., Longo, S., 2012a. Similarity solutions for spreading of a two-dimensional non-Newtonian gravity current in a porous layer. Journal of Non-Newtonian Fluid Mechanics 177–178, 46–53, http://dx.doi.org/10.1016/j.jnnfm.2012.04.003.

Di Federico, V., Archetti R., Longo S., 2012b. Spreading of axisymmetric non-Newtonian power-law gravity currents in porous media. Journal of Non-Newtonian Fluid Mechanics 189-190, 31–39, http://dx.doi.org/10.1016/j.jnnfm.2012.10.002.

Di Federico, V., Ciriello, V., 2012. Generalized Solution for 1-D non-Newtonian flow in a porous domain due to an instantaneous mass injection. Transport in Porous Media 93, 63–77, http://dx.doi.org/10.1007/s11242-012-9944-9.

Di Federico, V., Zhang, Y.-K., 1999. Solute transport in heterogeneous porous media with long-range correlations. Water Resources Research 35 (10), 3185–3191.

Jordan, P.M., Puri, P., 2003. Stokes' first problem for a Rivlin–Ericksen fluid of second grade in a porous half-space. International Journal of Non-Linear Mechanics 38 (7), 1019–1025.

Mathunjwa, J.S., Hogg, A.J., 2007. Freely draining gravity currents in porous media: dipole self-similar solutions with and without capillary retention. European Journal of Applied Mathematics 18, 337–362.

Pascal, H., 1991a. On non-linear effects in unsteady flows through porous media. International Journal of Non-Linear Mechanics 26 (2), 251–261.

Pascal, H., 1991b. On propagation of pressure disturbances in a non-Newtonian fluid flowing through a porous medium. International Journal of Non-Linear Mechanics 26 (5), 475–485.

Pascal, H., Pascal, F., 1985. Flow of non-Newtonian fluid through porous media. International Journal of Engineering Sciences 23 (5), 571–585.

Pascal, H., Pascal, F., 1990. On some self-similar flows of non-Newtonian fluids through a porous medium. Studies in Applied Mathematics 82, 1–12.

Pascal, J.P., Pascal, H., 1993. Similarity solutions to gravity flows of non-Newtonian fluids through porous media. International Journal of Non-Linear Mechanics 28 (2), 157–167.

Pearson, J.R.A., Tardy, P.M.J., 2002. Models of non-Newtonian and complex fluids through porous media. Journal of Non-Newtonian Fluid Mechanics 102 (2), 447–473.

Puri, P., Jordan, P.M., 2006. On the steady shear flow of a dipolar fluid in a porous half-space. International Journal of Engineering Science 44, 227–240.

Savins, J.G., 1969. Non-Newtonian flow through porous media. Industrial & Engineering Chemistry Research 6 (10), 18–47.

Shenoy, A.V., 1995. Non-Newtonian fluid heat transfer in porous media. Advances in Heat Transfer 24, 102–190.

Sochi, T., 2010. Non-Newtonian flow in porous media. Polymer 51 (22), 5007–5023.

Sullivan, S.P., Gladden, L.F., Johns, M.L., 2006. Simulation of power-law fluid flow through porous media using lattice Boltzmann techniques. Journal of Non-Newtonian Fluid Mechanics 133, 91–98.

Takagi, D., Huppert, H.E., 2008. Viscous gravity currents inside confining channels and fractures. Physics of Fluids 20, 023104.

Teeuw, D., Hesselink, F.T., 1980. Power-law flow and hydrodynamic behavior of biopolymer solutions in porous media. In: Proceedings of Fifth International Symposium on Oilfield and Geothermal Chemistry, SPE Paper 8982, pp. 73–86.

Yilmaz, N., Bakhtiyarov, A.S., Ibragimov, R.N., 2009. Experimental investigation of Newtonian and non-Newtonian fluid flows in porous media. Mechanics Research Communications 36 (5), 638–641.